

## An experimental and simulation study of the role of thermal effects on variability in TiN/Ti/HfO<sub>2</sub>/W resistive switching nonlinear devices

D. Maldonado<sup>a</sup>, C. Aguilera-Pedregosa<sup>a</sup>, G. Vinuesa<sup>b</sup>, H. García<sup>b</sup>, S. Dueñas<sup>b</sup>, H. Castán<sup>b</sup>, S. Aldana<sup>a</sup>, M.B. González<sup>c</sup>, E. Moreno<sup>d</sup>, F. Jiménez-Molinos<sup>a</sup>, F. Campabadal<sup>c</sup>, J.B. Roldán<sup>a,\*</sup>

<sup>a</sup> Departamento de Electrónica y Tecnología de Computadores, Universidad de Granada, Facultad de Ciencias, Avd. Fuentenueva s/n, 18071 Granada, Spain

<sup>b</sup> Departamento de Electrónica, Universidad de Valladolid, Paseo de Belén 15, 47011 Valladolid, Spain

<sup>c</sup> Institut de Microelectrónica de Barcelona, IMB-CNM (CSIC), Carrer dels Til·lers s/n, Campus UAB, 08193 Bellaterra, Spain

<sup>d</sup> Department of Electromagnetic Field, Czech Technical University in Prague, Faculty of Electrical Engineering, CTU, Technická 2, 166 27, Prague 6 Dejvice, Czech Republic

### ARTICLE INFO

#### Article history:

Received 15 February 2022

Received in revised form 27 April 2022

Accepted 19 May 2022

Available online xxx

#### Keywords:

Resistive switching memory

RRAM

Temperature characterization

Simulation

Variability

Modeling

Kinetic Monte Carlo

Series resistance

### ABSTRACT

An in-depth simulation and experimental study has been performed to analyze thermal effects on the variability of resistive memories. Kinetic Monte Carlo (kMC) simulations, that reproduce well the nonlinearity and stochasticity of resistive switching devices, have been employed to explain the experimental results. The series resistance and the transition voltages and currents have been extracted from devices based on the TiN/Ti/HfO<sub>2</sub>/W stack we have fabricated and measured at temperatures ranging from 77 K to 350 K. We observed that the variability for all the magnitudes analyzed was much higher at low temperatures. In the kMC simulations, we obtained conductive filaments (CFs) with less compactness at low temperatures. This led us to explain the higher variability, based on the variations of the CF morphology and density seen at low temperatures.

© 2022 The Authors. Published by Elsevier Ltd. This is an open access article under the CC BY-NC-ND license (<http://creativecommons.org/licenses/by-nc-nd/4.0/>).

### 1. Introduction

Resistive memories are being studied because of their outstanding properties for applications such as non-volatile memories, neuromorphic computing and hardware cryptography [1–5]. These resistive switching (RS) devices have shown good endurance [6], retention, low power consumption, full compatibility with CMOS technology and capability of 3D stack fabrication [1–5].

In what is related to non-volatile memory applications, different embedded solutions have been proposed to include these devices in integrated circuits (ICs) [7]. RRAM non-volatile applications (storage class memory) operate faster than currently dominant Flash devices and require less switching power. These devices, that belong to a greater group known as memristors [3,8,9], show a great potential for neuromorphic engineering purposes [10–20]. In this context, vector-matrix and matrix-vector multiplication circuits can be easily built with RS devices in an analog approach by implementing crossbar arrays. These structures can be used to accelerate large-scale data processing

systems, as it is the case of artificial neural networks and spiking neural networks, the latter encoding the information in the time domain by means of spikes [5,21]. Another application based on resistive switching devices that is gaining momentum consists in the fabrication of circuits to generate random numbers and implement physical unclonable functions [22–27].

Prior to the full introduction of this technology in the massive electronics industry, different issues have to be addressed, such as the cycle-to-cycle (C2C) variability that is inherent to RRAMs due to the stochasticity linked to resistive switching [28–35]. In devices with filamentary conduction, C2C variability is connected to the morphology of the conductive filament (CF) that shorts the electrodes to change the device resistance state [5,36,37]. In each resistive switching cycle, the CF is created (set process) to lead the device to the low resistance state and ruptured (reset process), leading the device to the high resistance state.

The accurate description of variability needs a clear view of the physical mechanisms that stand behind RS operation. Kinetic Monte Carlo simulation has been shown to be very useful for this purpose [32,33,36,38–41]. In addition, compact modeling can be a good option to account for variability in the circuit simulation context [8,29,42–50].

\* Corresponding author.

E-mail address: [jroldan@ugr.es](mailto:jroldan@ugr.es) (J.B. Roldán).

In this work, we deal with the study of resistive switching at low temperatures from the experimental and simulation viewpoints. In particular, we have focused on the relation between temperature and variability. Although resistive switching is an intrinsically stochastic process [51,52] where oxygen vacancies and ions, and metal species can diffuse and be involved in the device switching events [53], the influence of temperature on resistive switching has been shown experimentally [54–56] and comprehensively modeled [42,47,50] and simulated using kinetic Monte Carlo algorithms [38–40]. From this viewpoint, we have studied devices based on the TiN/Ti/HfO<sub>2</sub>/W stack that show filamentary resistive switching and a typical valence change memory (VCM) bipolar behavior [38,57–60] where the electric field direction plays an important role in the processes that lead to resistive switching [3,38,40,57]. Using the experimental data obtained at different temperatures as starting point, we have analyzed them with advanced numerical techniques to extract the series resistance [61–65] and the reset and set transition voltages and currents. The results are analyzed and compared to state-of-the-art kMC simulations to shed light on the physics behind the low temperature RS behavior. The comparison of experimental and simulated data is essential to unveil RS physics due to the complex, nonlinear and stochastic mechanisms that lie behind the RS phenomenon [29,38,43]. The conclusions drawn can be used to develop the basis of variability models to complement physical simulations and compact models that are extremely necessary for device design and circuit simulation. Variability is essential in this type of devices [29,66] and even if the modeling is devoted to keep circuits including these devices within correct operation parameters, it is important to highlight the potential of this variability when systems are built in an interdisciplinary physics context to take advantage of the constructive role of noise. As it is well known, noise can induce more ordered regimes, enhance the coherence degree of different systems (among them neuronal ones), increase the gain and signal-to-noise ratio at different system output...; moreover, noise plays a vital role in stochastic resonance phenomena, stochastic resonant activation and noise enhanced stability [29,67–78].

All these aspects are addressed as follows: in Section 2, we introduce the fabrication and measurement details; in Section 3, the simulation tools are described and in Section 4, the main results are summarized. Finally, the conclusions are drawn in Section 5.

## 2. Device fabrication and measurement setup

The resistive memories employed here were metal-insulator-metal structures fabricated on N-type ( $\rho = 4 \text{ m}\Omega \cdot \text{cm}$ ) silicon wafers. The top metal electrode is made of a bilayer stack (200 nm TiN/10 nm Ti) and the bottom metal (50 nm W) was deposited on a Ti adhesion layer (20 nm-thick) on a silicon substrate. The electrical contact to the W layer is made by Al-metallizing the Si wafer back. The insulator material is a 10 nm-thick HfO<sub>2</sub> dielectric film grown by atomic layer deposition. A detailed description of the fabrication process is given in [58].

The experimental measurements were carried out using a Hewlett-Packard Semiconductor Parameter Analyzer 4155B to perform the current-voltage (I-V) measurements. The W electrode (bottom electrode) was grounded, and the voltage was applied to the top electrode. Prior to the switching measurements, the samples underwent an electroforming process at room temperature using a compliance current of 0.2 mA to prevent irreversible oxide breakdown. After the forming process was carried out, the device was first cooled in darkness to the liquid nitrogen temperature ( $\sim 77 \text{ K}$ ) using an Oxford Instruments cryostat (model DM1710). The RS cycles were measured at several temperatures (77 K, 100 K, 125 K, 150 K, 200 K, 225 K, 250 K, 275 K, 300 K, 325 K, and 350 K) starting from 77 K and increasing then the temperature. We waited 20 min at each temperature before starting the measurements to ensure thermal stability. An Oxford Instruments temperature controller (model ITC 503) was used to monitor and control the

temperature during the measurements. One hundred complete RS cycles, including set and reset processes, were measured for each temperature. Ramped voltage signals with 25 mV step were employed in I-V measurements with a slope of about 0.4 V/s in the voltage intervals [0, 0.8 V] and [0,  $-1.2 \text{ V}$ ] without current limitation. All the equipment was connected to a computer via GPIB interface and controlled using Agilent VEE software.

Some of the I-V curves obtained are shown in Fig. 1 for different temperatures [58]. The complete set of curves is given in the supplementary information, see Fig. S1. The measurements at the different temperatures were carried out on one device. The devices studied here have been analyzed previously (see Refs. [79–82]). These results show that the device-to-device variability is clearly lower than the variations with temperature that we present here. In addition, after the forming process was performed, several I-V cycles were measured at room temperature to observe the switching behavior. After a proper operation was observed, the device was cooled. However, the 100 RS cycles at 300 K were recorded when increasing the temperature from 77 K, and after having measured 100 cycles at 77, 100, 125, 150, 200, 225, 250, and 275 K. The results obtained when measuring the 100 cycles at 300 K were similar to those obtained before cooling the device, so we can conclude that no degradation appeared after the low temperature measurements.

Both, the set and reset processes are highly influenced by the temperature. The set voltage decreases as the temperature is increased. This result makes sense since the physical mechanisms behind RS are thermally activated [36,50]; therefore, a threshold temperature is needed to trigger the processes that lead to the CF formation. As a consequence, the lower the ambient temperature the higher the voltage needed to reach this threshold temperature in the RS active device region by means of Joule heating.

## 3. Simulation description

A kinetic Monte Carlo simulation tool was utilized to study the devices reported in the previous section in a 3D simulation domain. Both set and reset processes were analyzed in successive RS cycles. The features of this simulator are thoroughly explained in Refs. [38,40].

The CFs created and ruptured in the RS operation are formed by a high concentration of oxygen vacancies [3,38,57]. The drift of oxygen ions due to the electric field favors the presence of oxygen vacancies which are positively charged. Some electrons (localized in the d-orbitals of the cation sublattice) could compensate the unbalanced charge generated in the dielectric, leading to a change of the

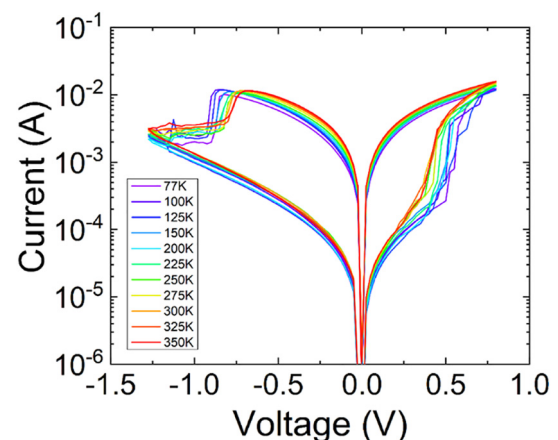


Fig. 1. Experimental I-V curves of the devices under study. One hundred complete RS cycles, including set and reset processes, are measured and analyzed for each temperature.

valence state of the transition metal cations; that is why these devices are known as valence change memories [57].

The 3D Poisson and heat differential equations (the latter given in Eq. 1) are considered for each time step to calculate temperatures and electric fields.

$$\dot{q} = -\nabla[k_{th}(x,y,z)\nabla T(x,y,z)] \quad (1)$$

where  $T$  is the temperature,  $k_{th}$  the thermal conductivity and  $\dot{q}$  stands for the heat generation rate. The physical mechanisms involved in RS are randomly activated using a kMC algorithm based on the Transition State Theory [33] and the temperature and electric field distributions.

The calculation of the transition rates is performed by means of the transition state theory through Eq. (2):

$$\Gamma = \nu \exp\left(-\frac{E_A}{k_B T}\right) \quad (2)$$

where  $\Gamma$  stands for the transition rate,  $\nu$  is the vibration constant of the particle,  $E_A$  is the activation energy (the energy barrier height for the process involved),  $k_B$  is the Boltzmann constant and  $T$  is the temperature [33]. The activation energy values employed to calculate the transitions rates of the different physical mechanisms are those given in [38]. A kMC tool is to our knowledge the best option to analyze theoretically the variability and random operation of resistive memories.

If a physical mechanism depends on the electric field, the activation energy is reduced using the local value of the electric field [38]. The relation between the transition rates of the mechanisms involved, the electric field and the temperature is exponential (Eq. (2)); therefore, nonlinear relations are expected in the operation of these devices, which is the usual case in redox-based devices such as those used in the present work. See that although variability is naturally obtained in the context of a kMC simulation tool, a refined focus would be needed to analyze the role of thermal noise in resistive switching, mostly in the reset transition. In this respect, we call the reader's attention to the fact that an approach based on the Fokker-Planck equation (since fluctuations are taken into consideration explicitly) could help to explain the nonlinear relaxation from the initial nonequilibrium distribution of internal state variables towards equilibrium. In a recently published work [83], a good description of the development of a framework for a resistive switching device stochastic behavior was presented. The devices (which are complex stochastic multistable systems, characterised by nonlinear relaxation phenomena and stochastic switching mechanisms [84,85]) operation in relation to the inherent stochasticity is expressed by the Langevin equation which is known to be the model of overdamped Brownian motion.

In order to analyze the heat flux, another simulation tool is employed with a homogenous metallic-like CF of cylindrical and truncated-cone shapes. In particular, we make use of a simulator described in [34,86]. Since the devices employed here are different to the ones employed in Refs. [34,86], we have changed the corresponding physical parameters, see Table S1 in the supplementary information. The heat generation rate ( $\dot{q}$ ) (Eq. (1)) can be obtained making use of the electrical conductivity and the electric field distribution in the CF, a linear metallic-like increase of the CF resistivity with temperature is assumed (the temperature coefficient is  $\alpha_T = 0.001 \text{ K}^{-1}$ ) [86].

#### 4. Results and discussion

The series resistance ( $R_{series}$ ) extraction technique is described in Fig. 2. The RRAM applied voltage ( $V_{applied}$ ) is reduced to account for the effects of the series resistance  $V_N = V_{Applied} - R_{series} * I_{Measured}$ , and the modified I-V curve ( $I_{Measured}-V_N$ ) is obtained (light colors in Fig. 2) [61,64]. By changing the  $R_{series}$  value, different modified I-V curves are obtained. A vertical modified I-V is searched to extract the corresponding series resistance; in doing so, other parameters such as the transition voltages for the set and reset processes can be obtained, see Fig. 2.

We have applied an automatic process to extract  $R_{series}$  in the whole set of I-V curves measured. The distributions (the values obtained from the 100 I-V curves at each temperature) are plotted for the different temperatures considered (Fig. 3). See that the lower the temperature the more spread out is the  $R_{series}$  distribution (higher variability). The standard deviation of the distributions for each temperature is shown in the inset. There is a clear dependence on the temperature (Table 1). This behavior can be explained by means of physical simulations that account for the stochasticity and nonlinearity of these devices, as will be shown below.

The series resistance values at room temperature are in the order of those reported in [61]. As explained there, the  $R_{series}$  accounts for the contribution of the electrodes, the different metal lines and the CF remnants produced in the resistive switching operation. At temperatures below 150 K the series resistance variability increases significantly. Note that temperature does not affect much the central series resistance values, but variability is seriously affected.

The cumulative distribution functions for the transition voltages for the set and reset processes, and the corresponding transition currents are given in Fig. 4. The transition currents for set,  $I_{TS}$ , and for reset,  $I_{TR}$ , are the currents that correspond to the transition voltages in the modified I-V curve. See that, again, we have more spread out  $V_{TS}$  and  $V_{TR}$  distributions for the lower temperatures.

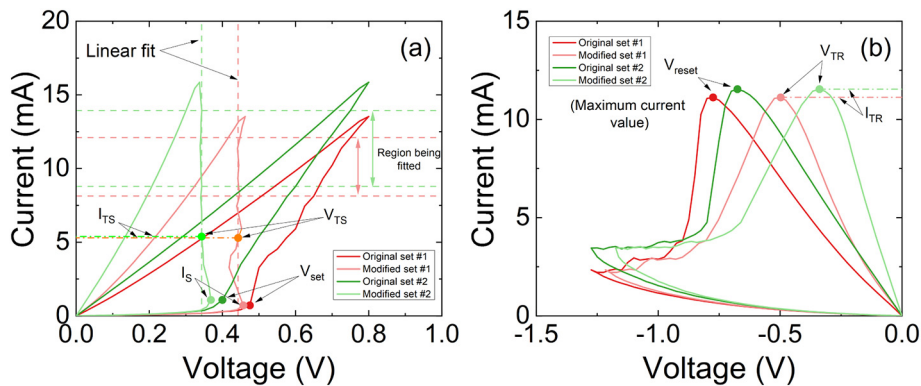


**Fig. 2.** Experimental current versus voltage for the devices under study. a) Original (dark green and dark red) and modified (light green and light red) set I-V curves employed for the series resistance extraction. The series resistance values for curves #1 (red) and #2 (green) are 24.9 Ohm and 29.1 Ohm, respectively, and were obtained following the methodology described in [61]. b) Original (dark green and dark red) and modified (light green and light red) reset I-V curves using the same series resistance values. (For interpretation of the references to colour in this figure legend, the reader is referred to the web version of this article.)



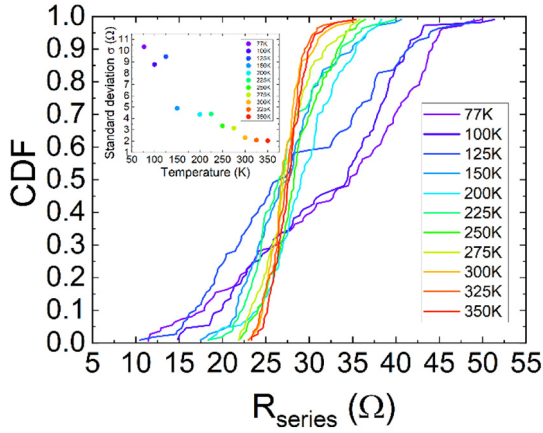


**Fig. 3.**  $R_{series}$  cumulative distribution functions in the RS series extracted measured for each temperature. Inset: series resistance standard deviation versus temperature for the measured distributions (see Table 1).

**Table 1**  
 $R_{series}$  standard deviation for the distributions obtained for each temperature.

Temperature (K)	Standard deviation (Ohms)
77	10.3
100	8.7
125	9.4
150	4.9
200	4.3
225	4.4
250	3.3
275	3.1
300	2.2
325	2.0
350	2.0

The  $I_{TS}$  differences with temperature are bigger since the set threshold voltage is obtained in the vertical section of the modified set I-V curve. Therefore, a wide range of  $I_{TS}$  values can be obtained for the

points that correspond to  $V_{TS}$ . This is not the case of  $I_{TR}$ . In the whole range of temperatures studied quite similar values of the absolute value of  $V_{TS}$  and  $V_{TR}$  are obtained, as it was the case in [61].

The behavior of the transition voltages and currents highlighted above can better be seen in Fig. 5. The clusters are more spread out at low temperatures. The data of  $I_{TR}$  versus  $V_{TR}$  (Fig. 5b) show a concentrated point cloud at high temperatures, nevertheless the areas covered by the clouds increase as temperature drops due to an increased variability. Similar results are seen for the data corresponding to the set process, taking the  $I_{TS}$  variation commented above into account.

We have tried to shed some light on the results presented by means of kMC simulations. A simulator tuned for these devices [38] allowed us to study both set and reset processes at different temperatures. In doing so, the CF compactness and density were calculated, see Fig. 6.

It can be seen that the reset (Fig. 6A and Fig. 6C) and set (Fig. 6B and Fig. 6D) processes were delayed (in terms of the applied voltage) at low temperature, as found experimentally. In relation to this, it was found that the CF compactness is lower at low temperatures (see the low level of oxygen vacancies with 6 and 5 neighbors in Fig. 6C and D in comparison with Fig. 6A and B respectively) due to the general freezing of the physical mechanisms (mostly thermally activated, see Eq. (2)) involved in the resistive switching process [38], which leads to a more fragile (less compact) filament. In line with this result, we calculated the CF density at 77 K during a reset process, which is considerably lower than at 300 K. The lower CF compactness leads to a higher variability, since the relative modification of the percolation paths (the resistive paths) that form the CF is easier when generation/recombination processes take place.

In order to describe correctly the heat flux in the surroundings of the conductive filament, we have made use of a finite differences simulator assuming homogeneous CFs of different shapes [34,86]. In the supplementary information the physical constants employed are given in Table S1 and the device structures within the simulation domain (SD) are shown in Fig. S2. By considering fixed CF shapes, a better analysis of the heat flux can be performed. We found that the relative lateral heat flux (lateral heat flux with respect to the total heat flux coming out of the conductive filament towards the electrodes and the surrounding insulator) does not

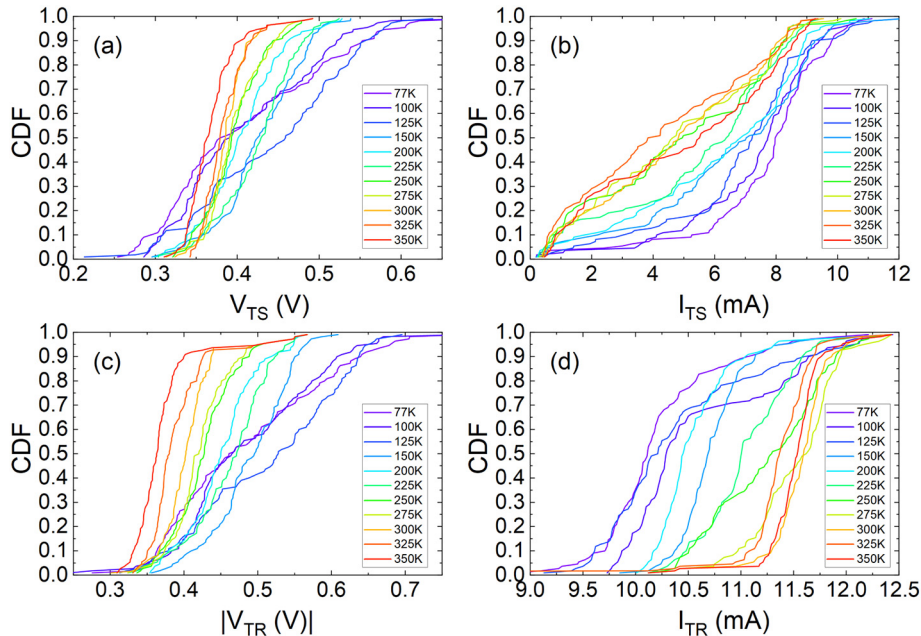


**Fig. 4.** Cumulative distribution functions for the parameters obtained in the  $R_{series}$  extraction procedure for each temperature. a) Transition voltages for the set ( $V_{TS}$ ) cycles, b) transition currents for the set ( $I_{TS}$ ) cycles, c) transition voltages for the reset ( $|V_{TR}|$ ) cycles, d) transition currents for the reset ( $I_{TR}$ ) cycles.

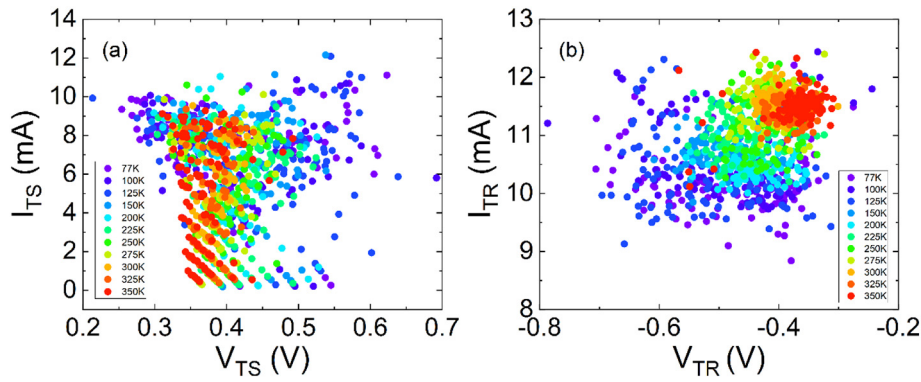


Fig. 5. a) Transition current versus transition voltage for the set cycles, b) transition current for reset versus transition voltage.

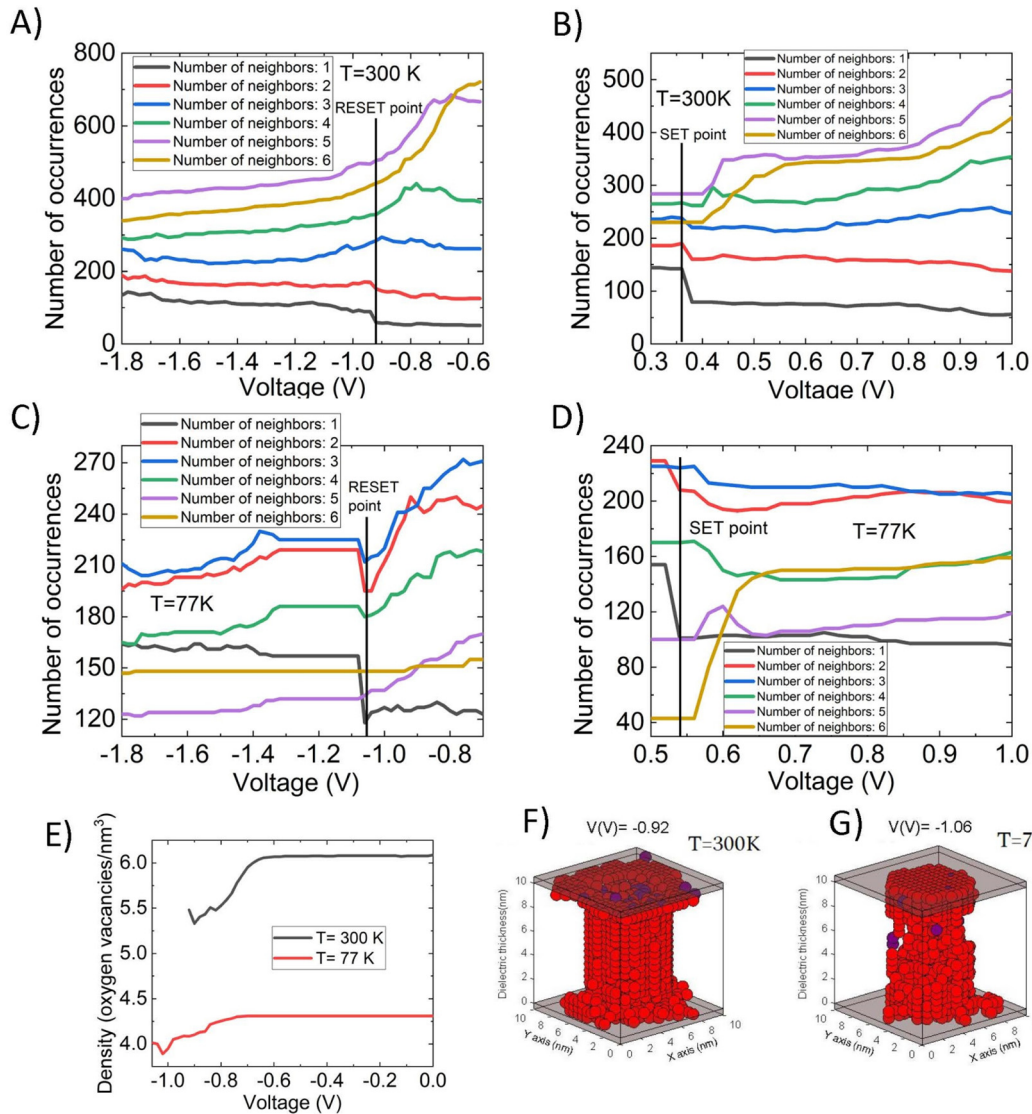
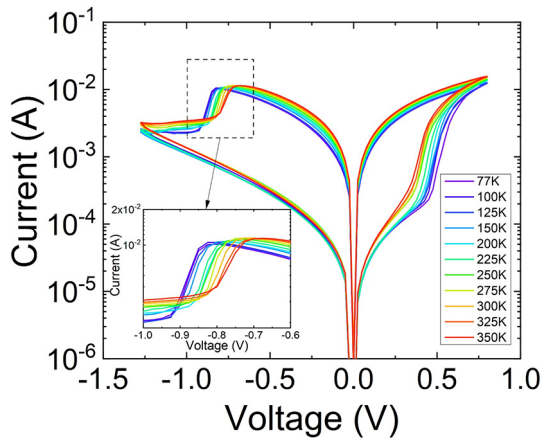


Fig. 6. Kinetic Monte Carlo simulation for the VCM devices under study for two different temperatures (300 K and 77 K). A) and B) represent the evolution of the number of oxygen vacancies with a certain number of neighbors around them for the RESET and SET processes respectively at 300 K. C) and D) represent the evolution of the number of oxygen vacancies with a certain number of neighbors around them for the RESET and SET processes respectively in a simulation where the ambient temperature was 77 K. E) This plot represents the evolution of the conductive filament density along a RESET process at both temperatures under consideration. For these simulations a previous forming process is performed at each temperature and several RS cycles. F) and G) correspond to a 3D conductive filament just before the rupture takes place in Fig. A) (300 K) and in Fig. C) (77 K) respectively.



**Fig. 7.** Experimental I-V curves for the set and reset processes at different temperatures. Each curve is obtained by calculating the mean of the 100 I-V curves measured at the same temperature. The inset shows a zoomed-in section of the reset process.

change much with temperature. The simulations were performed for a voltage of 0.4 V. Different configurations were employed: a cylindrical CF whose radius was 2.5 nm (the SD corresponds to Fig. S2c), a double-cone shaped CF with a 2 nm top radius and a central radius of 0.2 nm (the SD corresponds to Fig. S2a) and a truncated cone shape CF with a 2.5 nm high radius and a 1.5 nm low radius (the SD corresponds to Fig. S2b). Since the relative lateral heat flux does not change much for the temperature range analyzed, no great differences are expected in the CF geometry as the temperature changes; the differences observed experimentally are due just to the effects of temperature in the physical mechanisms in each case (affecting the transition rates calculation).

A direct consequence of the effects reported is seen in the shapes of the reset curves at different temperatures (see Fig. 7). The lower the temperature the more vertically the current decrease (see the inset in Fig. 7), i.e. a more abrupt transition takes place. This result is connected to the lower CF compactness (Fig. 6). As the reset process is triggered, the more porous CFs that are built at lower temperatures can be easily ruptured.

## 5. Conclusions

Valence change memories based on the TiN/Ti/HfO<sub>2</sub>/W stack have been fabricated and measured at different temperatures starting from 77 K. We have analyzed the experimental data to obtain the series resistance and the transition voltages and currents. The variability for all these magnitudes, highly linked to the resistive switching operation of these devices, significantly increases at low temperatures. To explain the results, we have employed different types of simulations, including kinetic Monte Carlo simulations, which reproduce well the nonlinearity and stochasticity of resistive switching devices. We have observed in our simulations less compactness in the conductive filaments at low temperatures. This leads to higher variations on the CF morphology and density that explains the low temperature results.

## CRedit authorship contribution statement

Conceptualization, J.B.R., F.C., S.D., H.C.; numerical method development, D.M., G.V., H.G., S.D., H.C.; simulations, S.A., C.A-P., E.M.; measurements and data curation, D.M., G.V., H.G., S.D., H.C.; original draft preparation, review and editing, J.B.R., F.J.-M., D.M., M.B. G. All authors have read and agreed to the published version of the manuscript.

## Declaration of competing interest

The authors declare that they have no known competing financial interests or personal relationships that could have appeared to influence the work reported in this paper.

## Acknowledgments

The authors thank the support of the Spanish Ministry of Science, Innovation and Universities and the FEDER program through projects TEC2017-84321-C4-1-R, TEC2017-84321-C4-2-R, TEC2017-84321-C4-3-R, and projects A.TIC.117.UGR18, B-TIC-624-UGR20 and IE2017-5414 funded by the Consejería de Conocimiento, Investigación y Universidad, Junta de Andalucía (Spain) and the FEDER program.

## Appendix A. Supplementary data

Supplementary data to this article can be found online at <https://doi.org/10.1016/j.chaos.2022.112247>.

## References

- [1] Pan F, Gao S, Chen C, Song C, Zeng F. Recent progress in resistive random access memories: materials, switching mechanisms and performance. *Mater Sci Eng.* 2014;83:1–59.
- [2] Lanza M, Wong HSP, Pop E, Ielmini D, Strukov D, Regan BC, et al. Recommended methods to study resistive switching devices. *Adv Electron Mater.* 2019;5:1800143.
- [3] Ielmini D, Waser R. Resistive switching: from fundamentals of nanoionic redox processes to memristive device applications. Wiley-VCH; 2015.
- [4] Lee JS, Lee S, Noh TW. Resistive switching phenomena: a review of statistical physics approaches. *Appl Phys Rev.* 2015;2:031303.
- [5] Spiga S, Sebastian A, Querlioz D, Rajendran B. Memristive devices for brain-inspired computing. Elsevier; 2020.
- [6] Lanza M, Waser R, Ielmini D, Yang JJ, Goux L, Suñe J, Kenyon AJ, Mehonic A, Spiga S, Rana V, Wiefels S, Menzel S, Valov I, Villena MA, Miranda E, Jing X, Campabadal F, Gonzalez M, Aguirre F, Palumbo F, Zhu K, Roldan JB, Puglisi FM, Larcher L, Hou T-H, Prodromakis T, Yang Y, Huang P, Wang T, Chai Y, Pey KL, Raghavan N, Duenas S, Wang T, Xia Q, Pazos S. Standards for the characterization of endurance in resistive switching devices. *ACS Nano.* 2021;15(11):17214–31. <https://doi.org/10.1021/acsnano.1c06980>.
- [7] Yu S, Jiang H, Huang S, Peng X, Lu A. Computing-in-memory chips for deep learning: recent trends and prospects. *IEEE Circuits Syst Mag.* 2021:31–56.
- [8] Corinto Fernando, Civalieri Pier Paolo, Chua Leon O. A theoretical approach to memristor devices. *IEEE J Emerging Sel Top Circuits Syst.* 2015;5(2):123–32.
- [9] Chua Leon O, Kang Sung Mo. Memristive devices and systems. *Proc IEEE.* 1976;64(2):209–23.
- [10] Yu S, Wu Y, Jeyasingh R, Kuzum D, Wong H-S. An electronic synapse device based on metal oxide resistive switching memory for neuromorphic computation. *IEEE Trans Electron Devices.* 2011;58(8):2729–37. <https://doi.org/10.1109/TED.2011.2147791>.
- [11] Ambrogio S, et al. Equivalent-accuracy accelerated neural-network training using analogue memory. *Nature.* 2018;558:60–7.
- [12] Hui F, Liu P, Hodge SA, Carey T, Wen C, Torrisi F, Thanuja D, Galhena L, Tomarchio F, Lin Y, Moreno E, Roldan JB, Koren E, Ferrari AC, Lanza M. In-situ observation of low-power Nano-synaptic response in graphene oxide using conductive atomic force microscopy. *Small.* 2021;2101100:1–8.
- [13] Merolla PA, Arthur JV, Alvarez-Icaza R, Cassidy AS, Sawada J, Akopyan F, Jackson BL, Imam N, Guo C, Nakamura Y, Brezko B, Vo I, Esser SK, Appuswamy R, Taba B, Amir A, Flickner MD, Risk WP, Manohar R, Modha DS. A million spiking-neuron integrated circuit with a scalable communication network and interface. *Science.* 2014;345:668–73.
- [14] Nandakumar SR, Rajendran B. Bio-mimetic synaptic plasticity and learning in a sub-500 mV Cu/SiO<sub>2</sub>/W. *Microelectron Eng.* 2020;226:111290.
- [15] Alibart F, Zamanidoost E, Strukov DB. Pattern classification by memristive crossbar circuits using ex situ and in situ training. *Nat Commun.* 2013;4:2072.
- [16] Prezioso M, Merrikh-Bayat F, Hoskins BD, Adam GC, Likharev KK, Strukov DB. Training and operation of an integrated neuromorphic network based on metal-oxide memristors. *Nature.* 2015;521:61–4.
- [17] Pérez-Bosch E, Romero-Zalaz R, Pérez E, Kalishettyhalli M, Reuben J, Schubert MA, Jiménez-Molinos F, Roldán JB, Wenger C. Toward reliable compact modeling of multilevel 1T-1R RRAM devices for neuromorphic systems. *Electronics.* 2021;10:645.
- [18] Zidan MA, Strachan JP, Lu WD. The future of electronics based on memristive systems. *Nat Electron.* 2018;1:22–9.
- [19] Romero-Zalaz R, Perez E, Jiménez-Molinos F, Wenger C, Roldán JB. Study of quantized hardware deep neural networks based on resistive switching devices, conventional versus convolutional approaches. *Electronics.* 2021;10:346.
- [20] Sakellaropoulos D, Bousoulas P, Nikas G, Arvanitis C, Bagakis E, Tsoukalas D. Enhancing the synaptic properties of low-power and forming-free HfO<sub>x</sub>/TaO<sub>y</sub>/HfO<sub>x</sub> resistive switching devices. *Microelectron Eng.* 2020;229:111358.
- [21] Sebastian A, Le Gallo M, Khaddam-Aljameh R, et al. Memory devices and applications for in-memory computing. *Nat Nanotechnol.* 2020;15:529–44.



- [22] Chen A. Utilizing the variability of resistive random access memory to implement reconfigurable physical unclonable functions. *IEEE Electron Device Lett.* Feb. 2015; 36(2):138–40.
- [23] Carboni R, Ielmini D. Stochastic memory devices for security and computing. *Adv Electron Mater.* 2019;5:1900198.
- [24] Lanza M, Wen C, Li X, Zanotti T, Puglisi FM, Shi Y, Saiz F, Antidormi A, Roche S, Zheng W, Liang X, Hu J, Duhm S, Zhu K, Hui F, Roldán JB, Garrido B, Wu T, Chen V, Pop E. Advanced data encryption using two-dimensional materials. *Adv Mater.* 2021; 2100185:1–12.
- [25] Wei Z. True random number generator using current difference based on a fractional stochastic model in 40-nm embedded ReRAM. 2016 IEEE international electron devices meeting (IEDM), San Francisco, CA; 2016. <https://doi.org/10.1109/IEDM.2016.7838349>. pp. 4.8.1–4.8.4.
- [26] Arumí D, Gómez-Pau A, Manich S, Rodríguez-Montañés R, Gonzalez MB, Campabadal F. Unpredictable bits generation based on RRAM parallel configuration. *IEEE Electron Device Lett.* 2019;40(2):341–4.
- [27] Yang B, Arumí D, Manich S, Gómez-Pau A, Rodríguez-Montañés R, Gonzalez MB, Campabadal F, Fang L. RRAM random number generator based on train of pulses. *Electronics.* 2021;10:1831.
- [28] Pérez E, Maldonado D, Acal C, Ruiz-Castro JE, Alonso FJ, Aguilera AM, et al. Analysis of the statistics of device-to-device and cycle-to-cycle variability in TiN/Ti/Al:HfO<sub>2</sub>/TiN RRAMs. *Microelectron Eng.* 2019;214:104–9.
- [29] Mikhaylov AN, Guseinov DV, Belov AI, Korolev DS, Shishmakova VA, Koryazhkina MN, Filatov DO, Gorshkov ON, Maldonado D, Alonso FJ, Roldán JB, Krichigin AV, Agudov NV, Dubkov AA, Carollo A, Spagnolo B. Stochastic resonance in a metal-oxide memristive device. *Chaos Solitons Fractals.* 2021;144:110723. <https://doi.org/10.1016/j.chaos.2021.110723>.
- [30] Alonso FJ, Maldonado D, Aguilera AM, Roldán JB. Memristor variability and stochastic physical properties modeling from a multivariate time series approach. *Chaos Solitons Fractals.* 2021;143:110461.
- [31] Chang SH, Lee JS, Chae SC, Lee SB, Liu C, Kahng B, Kim DW, Noh TW. “Occurrence of both unipolar memory and threshold resistance switching in a NiO film. *Phys Rev Lett.* 2009;102:026801.
- [32] Dirkmann S, Kaiser J, Wenger C, Mussenbrock T. Filament growth and resistive switching in hafnium oxide memristive devices. *ACS Appl Mater Interfaces.* 2018; 10(17):14857–68.
- [33] Guy J, Molas G, Blaise P, Bernard M, Roule A, Le Carval G, Delaye V, Toffoli A, Ghibaudo G, Clermidy F, De Salvo B, Perniola L. Investigation of forming, SET, and data retention of conductive-bridge random-access memory for stack optimization. *IEEE Trans Electron Devices.* 2015;62(11):3482–9.
- [34] Lanza M, Shi Y, Palumbo F, Aguirre F, Boyeras S, Yuan B, Yalon E, Moreno E, Wu T, Roldán JB. Temperature of conductive nanofilaments in hexagonal boron nitride based memristors showing threshold resistive switching. *Adv Electron Mater.* 2021;2100580. <https://doi.org/10.1002/aeml.202100580>.
- [35] González MB, Maestro-Izquierdo M, Poblador S, Zabala M, Campabadal F, González-Cordero G, et al. Synaptic devices based on resistive HfO<sub>2</sub> memristors. chapter in. Mem-elements for neuromorphic circuits with artificial intelligence applications. Elsevier; 2021.
- [36] Padovani A, Larcher L, Pirrotta O, Vandelli L, et al. Microscopic modeling of HfO<sub>x</sub> RRAM operations: from forming to switching. *IEEE Trans Electron Devices.* 2015; 62(6):1998–2006.
- [37] Villena MA, Roldán JB, Jiménez-Molinos F, Suñé J, Long S, Miranda E, Liu M. A comprehensive analysis on progressive reset transitions in RRAMs. *J Phys D Appl Phys.* 2014;7:205102.
- [38] Aldana S, García-Fernández P, Romero-Zalaz R, González MB, Jiménez-Molinos F, Gómez-Campos F, Campabadal F, Roldán JB. Resistive switching in HfO<sub>2</sub> based valence change memories, a comprehensive 3D kinetic Monte Carlo approach. *J Phys D Appl Phys.* 2020;53:225106 in press.
- [39] Menzel S, Kaupmann P, Waser R. Understanding filamentary growth in electrochemical metallization memory cells using kinetic Monte Carlo simulations. *Nanoscale.* 2015;7:12673.
- [40] Aldana S, Pérez E, Jiménez-Molinos F, Wenger C, Roldán JB. Kinetic Monte Carlo analysis of data retention in Al:HfO<sub>2</sub>-based resistive random access memories. *Semicond Sci Technol.* 2020;35:115012.
- [41] von Witzleben M, Fleck K, Funck C, Baumkötter B, Zuric M, Idt A, Breuer T, Waser R, Böttger U, Menzel S. Investigation of the impact of high temperatures on the switching kinetics of redox-based resistive switching cells using a high-speed nanoheater. *Adv Electron Mater.* 2017;3:1700294. <https://doi.org/10.1002/aeml.201700294>.
- [42] Huang P, Liu XY, Chen B, Li HT, Wang YJ, Deng YX, Kang JF. A physics-based compact model of metal-oxide-based RRAM DC and AC operations. *IEEE Trans Electron Devices.* 2013;60(12):4090–7.
- [43] Roldán JB, Alonso FJ, Aguilera AM, Maldonado D, Lanza M. Time series statistical analysis: a powerful tool to evaluate the variability of resistive switching memories. *J Appl Phys.* 2019;125:174504.
- [44] Chen P, Yu S. Compact modeling of RRAM devices and its applications in 1T1R and 1S1R Array design. *IEEE Trans Electron Devices.* Dec. 2015;62(12):4022–8.
- [45] Bocquet M, Deleruyelle D, Aziza H, Muller C, Portal JM, Cabout T, et al. Robust compact model for bipolar oxide-based resistive switching memories. *IEEE Trans Electron Devices.* 2014;61:674–81.
- [46] Picos R, Roldán JB, Chawa MMAI, García-Fernández P, Jiménez-Molinos F, García-Moreno E. Semiempirical modeling of reset transitions in unipolar resistive-switching based memristors. *Radioengineering J.* 2015;24:420–4.
- [47] Guan X, Yu S, Wong H-SPhilip. A SPICE compact model of metal oxide resistive switching memory with variations. *IEEE Electron Device Lett.* Oct. 2012;33(10):1405–1407.
- [48] Huang P, Zhu D, Chen S, Zhou Z, Chen Z, Gao B, et al. Compact model of HfO<sub>x</sub>-based electronic synaptic devices for neuromorphic computing. *IEEE Trans Electron Devices.* 2017;64(2):614–21.
- [49] Jiang Z, Wu Y, Yu S, L Yang, Song K, Karim Z, et al. A compact model for metal-oxide resistive random access memory with experiment verification. *IEEE Trans Electron Devices.* May 2016;63(5):1884–92. pp. 21.3.1–21.3.4.
- [50] Roldán JB, González-Cordero G, Picos R, Miranda E, Palumbo F, Jiménez-Molinos F, Moreno E, Maldonado D, Baldomá SB, Chawa MMoner AI, de Benito C, Stavrinides SG, Suñé J, Chua LO. On the thermal models for resistive random access memory circuit simulation. *Nanomaterials.* 2021;11:1261.
- [51] Surazhevsky IA, Demin VA, Ilyasov AI, Emelyanov AV, Nikiryu KE, Rylkov VV, Shchanikov SA, Bordanov IA, Gerasimova SA, Guseinov DV, Malekhonova NV, Pavlov DA, Belov AI, Mikhaylov AN, Kazantsev VB, Valenti D, Spagnolo B, Kovalchuk MV. Noise-assisted persistence and recovery of memory state in a memristive spiking neuromorphic network. *Chaos, Solitons Fractals.* 2021; 146:110890.
- [52] Mikhaylov A, Pimashkin A, Pigareva Y, Gerasimova S, Gryaznov E, Shchanikov S, Zuev A, Talanov M, Lavrov I, Demin V, Erokhin V, Lobov S, Mukhina I, Kazantsev V, Wu H, Spagnolo B. Neurohybrid memristive CMOS-integrated systems for biosensors and neuroprosthetics. *Front Neurosci.* 2020;14:358. <https://doi.org/10.3389/fnins.2020.00358>.
- [53] Andrade JMM, Rosário CMM, Menzel S, Waser R, Sobolev NA. Application of the quantum-point-contact formalism to model the filamentary conduction in Ta<sub>2</sub>O<sub>5</sub>-based resistive switching devices. *Phys Rev Appl.* 2022;17:034062.
- [54] Jiang Z, Wang Z, Zheng X, Fong S, Qin S, Chen H-Y, et al. Microsecond transient thermal behavior of HfO<sub>x</sub>-based resistive random access memory using a micro thermal stage (MTS). 2016 IEEE international electron devices meeting (IEDM); 2016. <https://doi.org/10.1109/IEDM.2016.7838465>. pp. 21.3.1–21.3.4.
- [55] Deshmukh S, Rojo MM, Yalon E, Vaziri S, Pop E. Probing self-heating in RRAM devices by sub-100 nm spatially resolved thermometry. 2018 76th device research conference (DRC); 2018. p. 1–2. <https://doi.org/10.1109/DRC.2018.8442187>.
- [56] Yalon E, Sharma AA, Skowronski M, Bain JA, Ritter D, Karpov IV. Thermometry of filamentary RRAM devices. *IEEE Trans Electron Devices.* 2015;62(9):2972–7. <https://doi.org/10.1109/TED.2015.2450760>.
- [57] Funck C, Menzel S. Comprehensive model of electron conduction in oxide-based memristive devices. *ACS Appl Electron Mater.* 2021;3:3674–92.
- [58] García H, Boo J, Vinuesa G, Ossorio O, Sahelices B, Dueñas S, et al. Influences of the temperature on the electrical properties of HfO<sub>2</sub>-based resistive switching devices. *Electronics.* 2021;10:2816.
- [59] Poblador S, González MB, Campabadal F. Investigation of the multilevel capability of TiN/Ti/HfO<sub>2</sub>/W resistive switching devices by sweep and pulse programming. *Microelectron Eng.* 2018;187–188:148.
- [60] Poblador S, Maestro-Izquierdo M, Zabala M, Gonzalez MB, Campabadal F. Methodology for the characterization and observation of filamentary spots in HfO<sub>x</sub>-based memristor devices. *Microelectron Eng.* 2020;223:111232.
- [61] Maldonado D, Aguirre F, González-Cordero G, Roldán AM, González MB, Jiménez-Molinos F, et al. Experimental study of the series resistance effect and its impact on the compact modeling of the conduction characteristics of HfO<sub>2</sub>-based resistive switching memories. *J Appl Phys.* 2021;130:054503.
- [62] Karpov V, Niraula D, Karpov I. Thermodynamic analysis of conductive filaments. *Appl Phys Lett.* 2016;109:093501.
- [63] Wouters DJ, Menzel S, Rupp JAJ, Hennen T, Waser R. On the universality of the I-V switching characteristics in non-volatile and volatile resistive switching oxides. *Faraday Discuss R Soc Chem.* 2019;1359–6640.
- [64] González MB, Maestro-Izquierdo M, Jiménez-Molinos F, Roldán JB, Campabadal F. Current transient response and role of the internal resistance in HfO<sub>x</sub>-based memristors. *Appl Phys Lett.* 2020;117:262902.
- [65] Fantini A, Wouters DJ, Degraeve R, Goux L, Pantisano L, Kar G, Chen Y-Y, Govoreanu B, Kittl JA, Altimime L, Jurczak M. Intrinsic switching behavior in HfO<sub>2</sub> RRAM by fast electrical measurements on novel 2R test structures. 4th IEEE international memory workshop, Milan; 2012. p. 1–4.
- [66] Maldonado D, Aldana S, Gonzalez MB, Jiménez-Molinos F, Ibáñez MJ, Barrera D, ... Roldán JB. Variability estimation in resistive switching devices, a numerical and kinetic Monte Carlo perspective. *Microelectron Eng.* 2022;257:111736.
- [67] Stassi R, Savasta S, Garziano L, Spagnolo B, Nori F. Output field-quadrature measurements and squeezing in ultrastrong cavity-QED. *New J Phys.* 2016; 18:123005.
- [68] Carollo A, Spagnolo B, Dubkov AA, Valenti D. On quantumness in multi-parameter quantum estimation. *J Stat Mech.* 2019;094010.
- [69] Guarcello C, Valenti D, Carollo A, B. Stabilization effects of dichotomous noise on the lifetime of the superconducting state in a long josephson junction. *Entropy.* 2015;17(5):2862–75.
- [70] Guarcello C, Valenti D, Spagnolo B, Pierro V, Filatella G. Anomalous transport effects on switching currents of graphene-based josephson junctions. *Nanotechnology.* 2017;28:134001.
- [71] Guarcello C, Valenti D, Spagnolo B, Pierro V, Filatella G. Josephson-based threshold detector for Lévy-distributed current fluctuations. *Phys Rev Appl.* 2019;11:044078.
- [72] Capala K, Padash A, Chechkin AV, Shokri B, Metzler R, Dybiec B. Lévy noise-driven escape from arctangent potential wells. *Chaos.* 2020;30:123103.
- [73] Lisowski B, Valenti D, Spagnolo B, Bier M, Gudowska-Nowak E. Stepping molecular motor amid Lévy white noise. *Phys Rev E.* 2015;91:042713.
- [74] Carollo A, Spagnolo B, Valenti D. Uhlmann curvature in dissipative phase transitions. *Sci Rep.* 2018;8:9852.
- [75] Spagnolo B, Cirone M, La Barbera A, de Pasquale F. Noise-induced effects in population dynamics. *J Phys Condens Matter.* 2002;14:2247.

- [76] Denaro G, Valenti D, Spagnolo B, Basilone G, Mazzola S, Zgozi SW, Aronica S, Bonanno A. Dynamics of two picophytoplankton groups in Mediterranean Sea: analysis of the deep chlorophyll maximum by a stochastic advection-reaction-diffusion model. *Plos One*. 2013;8:e66765.
- [77] Guarcello C, Valenti D, Spagnolo B. Phase dynamics in graphene-based Josephson junctions in the presence of thermal and correlated fluctuations. *Phys Rev B*. 2015;92:174519.
- [78] Carollo A, Valenti D, Spagnolo B. Geometry of quantum phase transitions. *Phys Rep*. 2020;838:1–72.
- [79] García H, Vinuesa G, Ossorio OG, Sahelices B, Castán H, Dueñas S, et al. Study of the set and reset transitions in HfO<sub>2</sub>-based ReRAM devices using a capacitor discharge. *Solid-State Electron*. 2021;183:108113.
- [80] García H, Dueñas S, Ossorio OG, Castán H. Current pulses to control the conductance in RRAM devices. *IEEE J Electron Devices Soc*. 2020;8:291–6.
- [81] García H, Domínguez LA, Castán H, Dueñas S. Control of the set and reset voltage polarity in anti-series and anti-parallel resistive switching structures. *Microelectron Eng*. 2019;216:111083.
- [82] García H, Ossorio OG, Dueñas S, Castán H. Controlling the intermediate conductance states in RRAM devices for synaptic applications. *Microelectron Eng*. 2019;215:110984.
- [83] Agudov V, Safonov AV, Krichigin AV, Kharcheva AA, Dubkov AA, Valenti D, Guseinov DV, Belov AI, Mikhaylov AN, Carollo A, Spagnolo B. Nonstationary distributions and relaxation times in a stochastic model of memristor. *J Stat Mech*. 2020.;024003.
- [84] Yakimov AV, Filatov DO, Gorshkov ON, Antonov DA, Liskin DA, Antonov IN, Belyakov AV, Klyuev AV, Carollo A, Spagnolo B. Measurement of the activation energies of oxygen ion diffusion in yttria stabilized zirconia by flicker noise spectroscopy. *Appl Phys Lett*. 2019;114:253506.
- [85] Filatov DO, Vrzheschch DV, Tabakov OV, Novikov AS, Belov AI, Antonov IN, et al. Noise-induced resistive switching in a memristor based on ZrO<sub>2</sub>(Y)/Ta<sub>2</sub>O<sub>5</sub> stack. *J Stat Mech Theory Exp*. 2019;2019(12):124026.
- [86] Maestro M, González MB, Jiménez-Molinos F, Moreno E, Roldán JB, Campabadal F. Unipolar resistive switching behavior in Al<sub>2</sub>O<sub>3</sub>/HfO<sub>2</sub> multilayer dielectric stacks: fabrication, characterization and simulation. *Nanotechnology*. 2020;31:135202.